

## STRUCTURAL BIOLOGY

# The 3.8 Å resolution cryo-EM structure of Zika virus

Devika Sirohi,<sup>1\*</sup> Zhenguo Chen,<sup>1\*</sup> Lei Sun,<sup>1</sup> Thomas Klose,<sup>1</sup> Theodore C. Pierson,<sup>2</sup> Michael G. Rossmann,<sup>1†</sup> Richard J. Kuhn<sup>1†</sup>

The recent rapid spread of Zika virus and its unexpected linkage to birth defects and an autoimmune neurological syndrome have generated worldwide concern. Zika virus is a flavivirus like the dengue, yellow fever, and West Nile viruses. We present the 3.8 angstrom resolution structure of mature Zika virus, determined by cryo-electron microscopy (cryo-EM). The structure of Zika virus is similar to other known flavivirus structures, except for the ~10 amino acids that surround the Asn<sup>154</sup> glycosylation site in each of the 180 envelope glycoproteins that make up the icosahedral shell. The carbohydrate moiety associated with this residue, which is recognizable in the cryo-EM electron density, may function as an attachment site of the virus to host cells. This region varies not only among Zika virus strains but also in other flaviviruses, which suggests that differences in this region may influence virus transmission and disease.

The current Zika virus (ZIKV) epidemic in the Americas is linked to a sudden increase in reported cases of congenital microcephaly and Guillain-Barré syndrome. This led the World Health Organization in February 2016 to declare “a public health emergency of

international concern” (1). ZIKV was first discovered in a sentinel rhesus monkey in the Zika valley of Uganda in 1947 (2). It was subsequently isolated from mosquitos in 1948 (2) and from humans in 1952 (3). It is a reemerging mosquito-transmitted virus that was relatively unknown

until 2007, when it caused a major epidemic on Yap Island in Micronesia (4), which was followed by outbreaks in Oceania in 2013 and 2014 (5). Since its introduction into Brazil in 2015 (6), the virus has spread rapidly across the Americas (7).

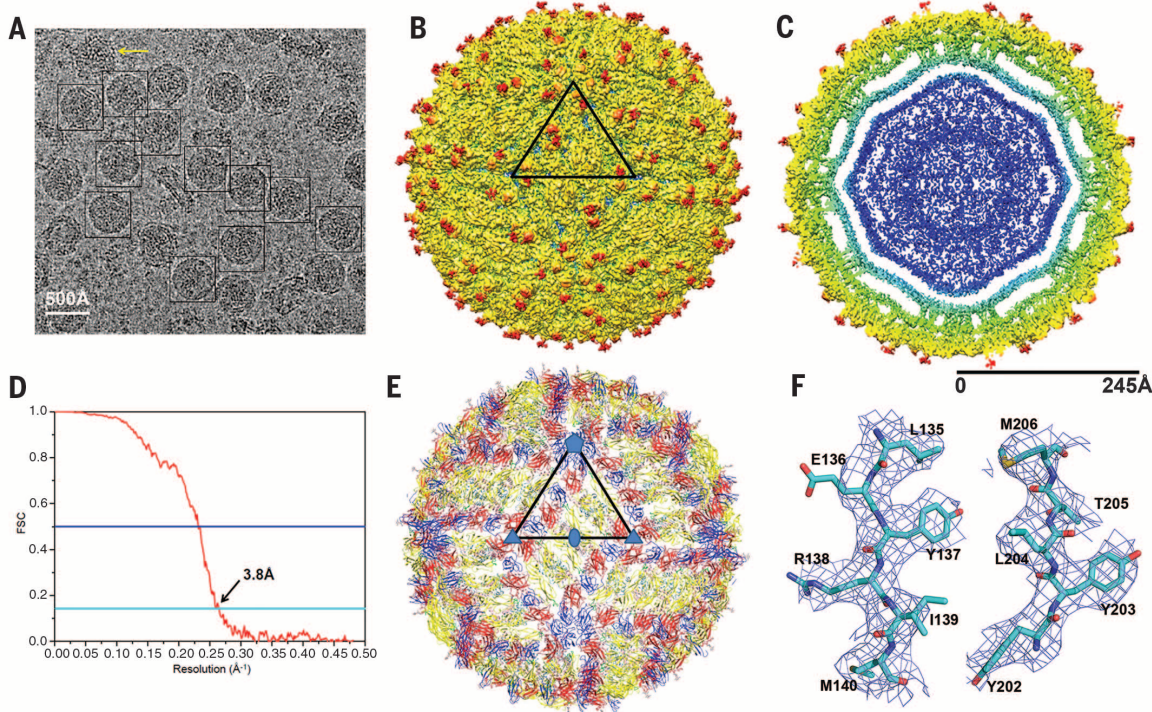
ZIKV belongs to the Flaviviridae family of positive-strand RNA viruses that includes human pathogens such as the mosquito-transmitted dengue virus (DENV), West Nile virus (WNV), Japanese encephalitis virus (JEV), yellow fever virus (YFV), and tick-borne encephalitic virus (8). ZIKV causes a rash and a febrile flulike illness in the majority of symptomatic individuals, but increasing evidence suggests a possibility of neurological abnormalities in developing fetuses (9, 10) and paralysis in infected adults (11). In addition to transmission by mosquitoes, ZIKV may be sexually (12, 13) and vertically transmitted (9, 10). The structure, tropism, and pathogenesis of ZIKV are largely unknown and are the focus of current investigations in an effort to address the need for rapid development of vaccines and therapeutics.

<sup>1</sup>Markey Center for Structural Biology and Purdue Institute for Inflammation, Immunology and Infectious Disease, Purdue University, West Lafayette, IN 47907, USA. <sup>2</sup>Viral Pathogenesis Section, Laboratory of Viral Diseases, National Institute of Allergy and Infectious Diseases, National Institutes of Health, Bethesda, MD 20892, USA.

\*These authors contributed equally to this work. †Corresponding authors. Email: mr@purdue.edu (M.G.R.); kuhn@purdue.edu (R.J.K.)

**Fig. 1. The cryo-EM structure of ZIKV at 3.8 Å. (A)** A representative cryo-EM image of frozen hydrated ZIKV, showing the distribution of virion phenotypes. Smooth, mature virus particles are shown enclosed in black boxes. A partially mature virus particle is identified by the yellow arrow. **(B)** A surface-shaded depth-cued representation of ZIKV, viewed down the icosahedral twofold axis. The asymmetric unit is identified by the black triangle. **(C)** A cross section of ZIKV showing the radial density distribution. Color coding in (B) and (C) is based on radii, as follows: blue, up to 130 Å; cyan, 131

to 150 Å; green, 151 to 190 Å; yellow, 191 to 230 Å; red, 231 Å and above. The region shown in blue fails to follow icosahedral symmetry, and therefore its density is uninterrupted, as is the case with other flaviviruses. **(D)** A plot of the Fourier shell correlation (FSC). Based on the 0.143 criterion for the comparison of two independent data sets, the resolution of the reconstruction is 3.8 Å. **(E)** The Cα backbone of the E and M proteins in the icosahedral ZIKV particle [same orientation as in (B)], showing the herringbone organization. The



color code follows the standard designation of E protein domains I (red), II (yellow), and III (blue). **(F)** Representative cryo-EM electron densities of several amino acids of the E protein. Cyan indicates carbon atoms; dark blue, nitrogen atoms; red, oxygen atoms; and yellow, sulfur atoms. Single-letter abbreviations for the amino acid residues are as follows: A, Ala; C, Cys; D, Asp; E, Glu; F, Phe; G, Gly; H, His; I, Ile; K, Lys; L, Leu; M, Met; N, Asn; P, Pro; Q, Gln; R, Arg; S, Ser; T, Thr; V, Val; W, Trp; and Y, Tyr.

Flaviviruses are enveloped viruses containing an RNA genome of about 11,000 bases complexed with multiple copies of the capsid protein, surrounded by an icosahedral shell consisting of 180 copies each of the envelope (E) glycoprotein (~500 amino acids) and the membrane (M) protein (~75 amino acids) or precursor membrane (prM) protein (~165 amino acids), all anchored in a lipid membrane. The genome also codes for seven non-structural proteins that are involved in replication, assembly, and antagonizing the host innate response to infection. During their life cycle, flavivirus virions exist in three major states—immature, mature, and fusogenic—which are non-infectious, infectious, and host membrane-binding states, respectively (8). The virus is initially assembled in the endoplasmic reticulum as a non-infectious “spiky” immature particle, consisting of 60 trimeric E:prM heterodimer spikes (14). Maturation into a “smooth” virus, consisting of 90 dimeric E:M heterodimers (15, 16), occurs in the low-pH environment of the trans-Golgi network through conformational changes of the surface glycoproteins and cleavage of prM into the pr peptide and M protein by the host protease furin. In the immature virus, the pr peptide protects the ~12-amino acid fusion loop on the E protein. Removal of the pr peptide during the maturation process exposes the fusion loop, priming the virus for low pH-mediated endosomal fusion (17). In addition to the aforementioned states, the structure of flavivirus virions can be influenced by temperature (18) and the efficiency of prM cleavage, resulting in a heterogeneous population of particles (19).

We report here the cryo-electron microscopy (cryo-EM) structure of the mature ZIKV at near-atomic resolution (3.8 Å) and compare it with the structure of other flaviviruses to provide a foundation for detailed analyses of the virology, antigenicity, and pathogenesis of this emerging threat to public health. ZIKV strain H/PF/2013, which was isolated from an infected patient during the 2013–2014 French Polynesia epidemic (20), was grown and purified from mammalian cells at 37°C. It was shown recently that the coding region of this strain has >99.9% amino acid identity to the strain that is currently circulating in Latin America (21). Low-passage Vero cells, derived from African green monkey kidney cells, were chosen for propagating the virus. To ensure a homogeneous population of virions suitable for single-particle reconstruction, virus was purified from Vero cells that overexpressed the host protease furin (Vero-furin). Vero-furin cells ( $10^9$ ) were infected with ZIKV at a multiplicity of infection of 0.1. The virus was harvested under conditions of low cytopathic effect and purified using polyethylene glycol 8000, 24% sucrose cushion ultracentrifugation, and a potassium tartrate (10 to 35%)-glycerol (7.5 to 26%) gradient, as previously described (17). The identity of the virus was verified by reverse transcription polymerase chain reaction (RT-PCR) and quantitative RT-PCR (22); the primer sequences are shown in table S1.

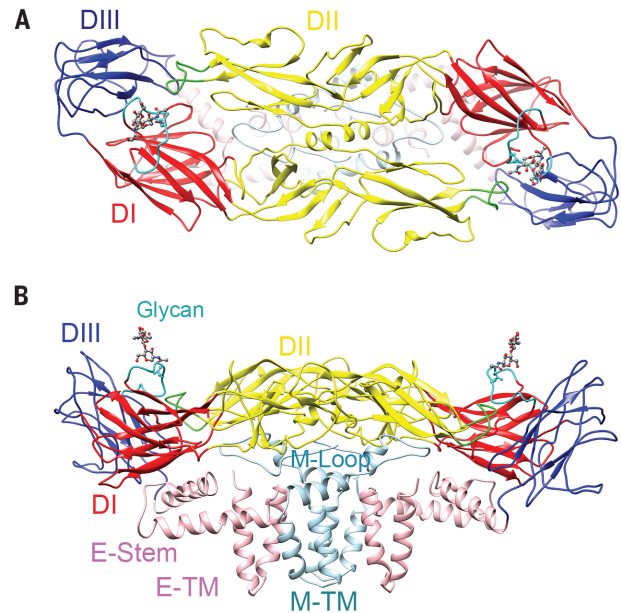
The ZIKV preparation was frozen onto lacey carbon EM grids and examined with an FEI

**Fig. 2. The structures of the ZIKV E and M proteins.**

(A) The E protein dimer is shown in ribbon form, viewed down the twofold axis. The color code follows the standard designation of E protein domains I (red), II (yellow) and III (blue). The underlying stem and transmembrane residues are shown (light pink). The fusion loop (green; fig. S1), the Asn<sup>154</sup> glycan (ball-and-stick representation), and the variable loop surrounding the Asn<sup>154</sup> glycan (cyan; residues 145 to 160) are shown.

(B) Side view of the (E-M)<sub>2</sub>, showing the three E ectodomains, as well as the E stem-transmembrane domains (pink) and the M loop and stem-transmembrane domains (light blue; TM, transmembrane). The E and M transmembrane domains are found within the lipid bilayer (Fig. 1C). All residues of M (1 to 75) and all but three residues of E (1 to 501) were identified in the density. The Asn<sup>154</sup> glycan from one monomer is labeled and can be seen projecting from the surface.

Titan Krios electron microscope equipped with a Gatan K2 Summit detector; a magnification of 14,000 in the “super-resolution” mode was used, resulting in a pixel size of 1.04 Å (Fig. 1A). The total exposure time for producing one image composed of 70 frames was 14 s and required a dose rate of 2 electrons Å<sup>-2</sup> s<sup>-1</sup>. A total of 2974 images were collected, and 64,518 particles were boxed using the automated Appion method (23). Non-reference two-dimensional (2D) classification was performed using the Relion program (24) to select 20,151 particles. The data set was split into two subsets according to the “gold standard” convention (25). The jspr program (26) was used for initial model generation, refinement of the orientation, and centering of the selected particles. After two rounds of 3D classification, 11,842 particles were used to generate a cryo-EM map at an average resolution of 4.2 Å. Application of soft masks improved the overall resolution to 3.8 Å, calculated using the 0.143 Fourier shell correlation criterion (25) (Fig. 1D). The structure of DENV2 serotype (16) was used as a starting point for model building. The atomic model was built manually using the program Coot (27) and refined with Phenix (28) and CNS (29). The final cryo-EM density was Fourier-analyzed. The resultant Fourier coefficients were used as targets for a crystallographic refinement. The final  $R_{\text{work}}$  and  $R_{\text{free}}$  were 34 and 34%, respectively (table S2). The map shows continuous density for the E and M polypeptide chains, and large side-chain densities are also visible in many cases, which was useful for sequence assignment. Except for the last three residues of E at its C terminus, all residues in both the E (residues 1 to 501) and M (residues 1 to 75) proteins were fitted into the density (Fig. 1E). A representative



volume of density is shown in Fig. 1F. Similar to other flaviviruses, the E protein of ZIKV consists of four domains: the stem-transmembrane domain that anchors the protein into the membrane and domains I, II, and III that constitute the predominantly β-strand surface portion of the protein (Fig. 2). The M protein consists of a loop at the N terminus (M loop or soluble M) and stem and transmembrane regions containing one and two helices, respectively, which anchor the M protein to the lipid bilayer (figs. S1 and S2).

The cryo-EM map shows that the mature ZIKV structure is similar to mature DENV (15, 16) and WNV structures (30) (Fig. 1). The radial distances of the core lipid bilayer and envelope ectodomains are similar to those of DENV2 (16) (Fig. 1C). A noticeable feature is the protruding density on the surface of the virus (red in Fig. 1, B and C), which is the glycan on the E protein. The E proteins exhibit the characteristic herringbone structure in the virion, in which there is one (E-M)<sub>2</sub> dimeric heterodimer located on each of 30 two-fold vertices and 60 (E-M)<sub>2</sub> dimeric heterodimers in general positions within the icosahedral protein shell (Fig. 1E). The root mean square deviation between equivalent Cα atoms of the E and M proteins of mature ZIKV and DENV is 1.8 Å. However, by far the biggest difference (up to 6 Å) between equivalent Cα atoms of these viruses is the region around the glycosylation sites (Asn<sup>154</sup> in ZIKV and Asn<sup>153</sup> in DENV) (Fig. 3). ZIKV has a single glycosylation site in the E protein (Asn<sup>154</sup>), whereas DENV is glycosylated at two sites within the E protein (Asn<sup>67</sup> and Asn<sup>153</sup>) (fig. S2). Dendritic cell-specific intercellular adhesion molecule 3-grabbing nonintegrin (DC-SIGN) and the mannose receptor are putative DENV receptors that

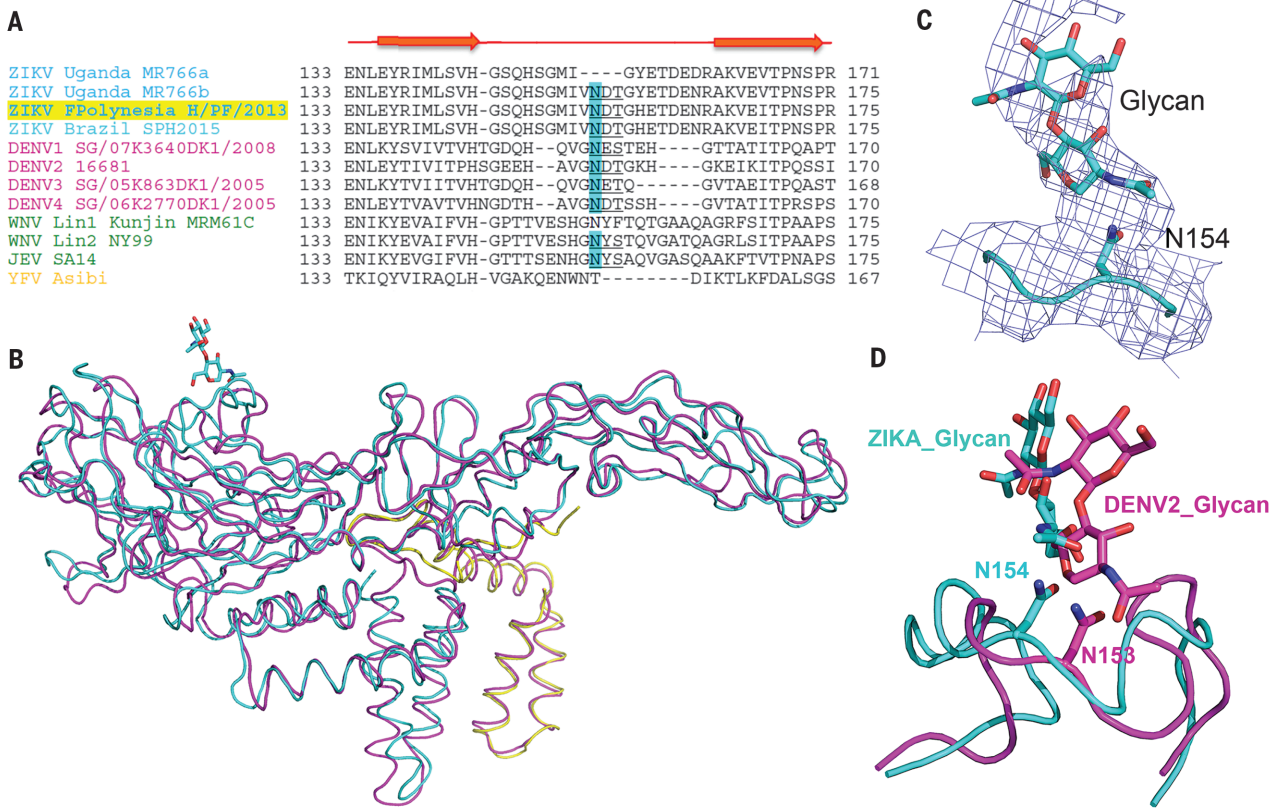


**Fig. 3. Comparison of the E protein of ZIKV with that of other flaviviruses.** (A) The region of the E protein of ZIKV strain H/PF/2013 (highlighted yellow) and other ZIKV strains is aligned to that of representative mosquito-transmitted flaviviruses. About 40 residues of domain I, centered on the Asn<sup>154</sup> glycosylation site, are compared. The conserved glycosylation site at Asn<sup>153–154</sup> is highlighted in blue. Red arrows represent secondary structures of ZIKV (sheets). The glycosylation motif N-X-S/T is underlined. The sequences for the flaviviruses were obtained from the Virus Pathogen Database and Analysis Resource. Virus strains for which structural information was available were chosen where possible. GenBank genome accession codes for these viruses are as follows: ZIKV Uganda MR766a, AY632535; ZIKV Uganda MR766b, KU720415; ZIKV FPPolynesia H/PF/2013, KJ776791; ZIKV Brazil SPH2015, KU321639; DENV1 SG/07K3640DK1/2008, Q0398255; DENV2 16681, NC001474;

DENV3 SG/05K863DK1/2005, EU081190; DENV4 SG/06K2270DK1/2005, Q0398256; WNV Lin1 Kunjin MRM61C, D00246; WNV Lin2 NY99, DQ211652; JEV SA14, D90194; and YFV Asibi, AY640589. The sequence of the original isolate (ZIKV MR766) varies based on the information source; it remains unclear whether this strain was glycosylated at N<sup>154</sup> at the time of isolation or whether the glycosylation was acquired during passage through mouse brain. The sequences were manually aligned based on the structures of ZIKV and DENV2. (B) Superposition of the Cα backbone of the ZIKV and DENV2 E and M proteins. The DENV2 proteins are shown in magenta, the ZIKV E protein is shown in cyan, and the ZIKV M protein is shown in yellow. (C) Electron density representing the glycan at Asn<sup>154</sup> in ZIKV. (D) Superposition of the loop region surrounding the glycosylation site (ZIKV, 144 to 166; DENV2, 144 to 161) that flanks the Asn<sup>154</sup> glycan in ZIKV (cyan) and the Asn<sup>153</sup> glycan in DENV2 (magenta).

bind to the glycans (31, 32). DC-SIGN was shown by cryo-EM to bind to the glycans at Asn<sup>67</sup> on two neighboring E proteins of the mature virion (31).

The structures of various flaviviruses alone and in complex with neutralizing antibodies (33) or cellular receptors (31) have been reported previously. These structures have demonstrated multiple mechanisms of antibody neutralization and receptor interactions. Carbohydrate moieties on the virus may be used for cell attachment and probably play a role in disease severity. For DENV, glycosylation at Asn<sup>67</sup> on the E protein is an attachment site for several cell types that have been shown to be relevant targets of infection in vivo (31, 32). Similarly, glycosylation at Asn<sup>154</sup> in WNV has been linked to neurotropism (34). These observations demonstrate the importance of glycosylation for the attachment of flaviviruses to cells. The carbohydrate densities for ZIKV and DENV2

are not coincident, and the conformation of their surrounding residues is different (Fig. 3). This region varies not only among ZIKV strains (35) but also in other flaviviruses, which suggests that differences in this region influence local virus structure and possibly dynamics (Fig. 3D). In part, this difference is because of an insertion of five residues in ZIKV relative to DENV (Fig. 3A), reflecting a highly variable region of the E protein. The glycan at E residue 154 is located on a loop that is adjacent to the fusion peptide in the neighboring E protein and may control solvent access to the fusion loop. The conserved fusion loop and the neighboring region is an epitope for numerous cross-reactive antibodies that vary considerably in potency and sensitivity to the presence of uncleaved prM on the virion (36). The differences discussed here may modulate the sensitivity of ZIKV to antibodies that bind the fusion

loop epitopes. Furthermore, this region may also be important for attachment to cellular lectin receptors. The differences shown here in E protein structure among ZIKV and other flaviviruses may govern cellular tropism and contribute to disease outcomes.

#### REFERENCES AND NOTES

- World Health Organization (WHO), *Zika Strategic Response Framework & Joint Operations Plan (January-June 2016)* (WHO, 2016).
- G. W. Dick, S. F. Kitchen, A. J. Haddow, *Trans. R. Soc. Trop. Med. Hyg.* **46**, 509–520 (1952).
- F. N. MacNamara, *Trans. R. Soc. Trop. Med. Hyg.* **48**, 139–145 (1954).
- M. R. Duffy et al., *N. Engl. J. Med.* **360**, 2536–2543 (2009).
- V. M. Cao-Lormeau et al., *Emerg. Infect. Dis.* **20**, 1085–1086 (2014).
- C. Zanluca et al., *Mem. Inst. Oswaldo Cruz* **110**, 569–572 (2015).
- European Center for Disease Prevention and Control (ECDC), *Rapid Risk Assessment: Zika Virus Disease Epidemic: Potential*

- Association with Microcephaly and Guillain–Barré Syndrome. Third Update, 23 February 2016 (ECDC, 2016).
8. B. D. Lindenbach, C. L. Murray, H.-J. Thile, C. M. Rice, in *Fields Virology*, D. M. Knipe, P. M. Howley, Eds. (Lippincott Williams & Wilkins, ed. 6, vol. 1, 2013), chap. 25, pp. 712–746.
  9. J. Mlakar et al., *N. Engl. J. Med.* **374**, 951–958 (2016).
  10. R. B. Martines et al., *MMWR Morb. Mortal. Wkly. Rep.* **65**, 159–160 (2016).
  11. V.-M. Cao-Lormeau et al., *Lancet* 10.1016/S0140-6736(16)00562-6 (2016).
  12. B. D. Foy et al., *Emerg. Infect. Dis.* **17**, 880–882 (2011).
  13. D. Musso et al., *Emerg. Infect. Dis.* **21**, 359–361 (2015).
  14. Y. Zhang et al., *EMBO J.* **22**, 2604–2613 (2003).
  15. R. J. Kuhn et al., *Cell* **108**, 717–725 (2002).
  16. X. Zhang et al., *Nat. Struct. Mol. Biol.* **20**, 105–110 (2013).
  17. I. M. Yu et al., *Science* **319**, 1834–1837 (2008).
  18. X. Zhang et al., *Proc. Natl. Acad. Sci. U.S.A.* **110**, 6795–6799 (2013).
  19. T. C. Pierson, M. S. Diamond, *Curr. Opin. Virol.* **2**, 168–175 (2012).
  20. C. Baronti et al., *Genome Announc.* **2**, e00500-14 (2014).
  21. A. Enfissi, J. Codrington, J. Roosblad, M. Kazanji, D. Rousset, *Lancet* **387**, 227–228 (2016).
  22. R. S. Lanciotti et al., *Emerg. Infect. Dis.* **14**, 1232–1239 (2008).
  23. G. C. Lander et al., *J. Struct. Biol.* **166**, 95–102 (2009).
  24. S. H. Scheres, *J. Struct. Biol.* **180**, 519–530 (2012).
  25. P. B. Rosenthal, R. Henderson, *J. Mol. Biol.* **333**, 721–745 (2003).
  26. F. Guo, W. Jiang, *Methods Mol. Biol.* **1117**, 401–443 (2013).
  27. P. Emsley, B. Lohkamp, W. G. Scott, K. Cowtan, *Acta Crystallogr. D Biol. Crystallogr.* **66**, 486–501 (2010).
  28. P. V. Afonine et al., *Acta Crystallogr. D Biol. Crystallogr.* **68**, 352–367 (2012).
  29. A. T. Brünger et al., *Acta Crystallogr. D Biol. Crystallogr.* **54**, 905–921 (1998).
  30. S. Mukhopadhyay, B. S. Kim, P. R. Chipman, M. G. Rossmann, R. J. Kuhn, *Science* **302**, 248 (2003).
  31. E. Pokidysheva et al., *Cell* **124**, 485–493 (2006).
  32. J. L. Miller et al., *PLOS Pathog.* **4**, e17 (2008).
  33. S. M. Lok, *Trends Microbiol.* 10.1016/j.tim.2015.12.004 (2015).
  34. D. W. Beasley et al., *J. Virol.* **79**, 8339–8347 (2005).
  35. O. Faye et al., *PLOS Negl. Trop. Dis.* **8**, e2636 (2014).
  36. S. Nelson et al., *PLOS Pathog.* **4**, e1000060 (2008).

#### ACKNOWLEDGMENTS

We thank X. de Lamballerie (Emergence des Pathologies Virales, Aix-Marseille Université, Marseille, France) and the European Virus Archive Goes Global (EVAg) for consenting to the use of the H/PF/2013 ZIKV strain for this study under a material transfer agreement with EVAg's partner, Aix-Marseille Université, and we thank M. S. Diamond (Washington University, St. Louis, MO, USA) for sending the virus. We acknowledge E. Frye for help with sequence alignments. We also acknowledge the use of the Purdue cryo-EM facility. We are grateful to W. Jiang for his jspr program, which was used to perform the anisotropic magnification corrections, and Y. Liu for providing help in submitting the Protein Data Bank (PDB) coordinates. The work presented in this report was funded by the National Institute of Allergy and Infectious Diseases of the NIH through grants R01AI073755 and R01AI076331 to M.G.R. and R.J.K. T.C.P was supported by the intramural program of the National Institute of Allergy and Infectious Diseases. Supporting information for this research is provided in the supplementary materials. The atomic coordinates and cryo-EM density maps for the mature ZIKV are available at the PDB and Electron Microscopy Data Bank under accession codes 5IRE and EMD-8116, respectively.

#### SUPPLEMENTARY MATERIALS

[www.sciencemag.org/content/352/6284/467/suppl/DC1](http://www.sciencemag.org/content/352/6284/467/suppl/DC1)  
Figs. S1 and S2  
Tables S1 and S2  
References (37, 38)  
4 March 2016; accepted 21 March 2016  
Published online 31 March 2016  
10.1126/science.aaf5316

#### EVOLUTIONARY GENETICS

# A beak size locus in Darwin's finches facilitated character displacement during a drought

Sangeet Lamichhaney,<sup>1</sup> Fan Han,<sup>1</sup> Jonas Berglund,<sup>1</sup> Chao Wang,<sup>1</sup> Markus Sällman Almén,<sup>1</sup> Matthew T. Webster,<sup>1</sup> B. Rosemary Grant,<sup>2</sup> Peter R. Grant,<sup>2</sup> Leif Andersson<sup>1,3,4\*</sup>

**Ecological character displacement is a process of morphological divergence that reduces competition for limited resources. We used genomic analysis to investigate the genetic basis of a documented character displacement event in Darwin's finches on Daphne Major in the Galápagos Islands: The medium ground finch diverged from its competitor, the large ground finch, during a severe drought. We discovered a genomic region containing the *HMGAA2* gene that varies systematically among Darwin's finch species with different beak sizes. Two haplotypes that diverged early in the radiation were involved in the character displacement event: Genotypes associated with large beak size were at a strong selective disadvantage in medium ground finches (selection coefficient  $s = 0.59$ ). Thus, a major locus has apparently facilitated a rapid ecological diversification in the adaptive radiation of Darwin's finches.**

**S**imilar species potentially compete for limited resources when they encounter each other through a change in geographical ranges. As a result of resource competition, they may diverge in traits associated with exploiting these resources (*1, 2*). Darwin proposed this as the principle of character divergence [now known as ecological character displacement (*3, 4*)], a process invoked as an important mechanism in the assembly of complex ecological communities (*5, 6*). It is also an important component of models of speciation (*6, 7*). However, it has been difficult to obtain unequivocal evidence for ecological character displacement in nature (*8, 9*). The medium ground finch (*Geospiza fortis*) and large ground finch (*G. magnirostris*) on the small island of Daphne Major provide one example where rigorous criteria have been met (*10*). Beak sizes diverged as a result of a selective disadvantage to medium ground finches with large beaks when food availability declined through competition with large ground finches during a severe drought in 2004–2005 (*11*).

Size-related traits can pose problems for the analysis of selection, and Darwin's finch beaks are no exception, as beak size and body size are strongly correlated ( $r = 0.7$  to  $0.8$ ) (*11*). We used a combination of multiple regression and selection differential analysis to investigate the 2004–2005 selection event. Statistically, these produced much stronger associations between

survival and beak size ( $S = -1.02$ ,  $P < 0.0001$ ) than between survival and body size ( $S = -0.67$ ,  $P < 0.05$ ). Thus, body size was possibly subject to selection, but beak size was a more important factor affecting the probability of survival independent of body size (*11, 12*). However, the genetic basis of the selected traits remains unknown. Beak dimensions and overall body size of the medium ground finch are highly heritable (*13*), but no gene(s) regulating body size have been identified. Furthermore, although some signaling molecules affecting beak dimensions in Darwin's finches have been identified (*14*), only one regulatory gene, *ALX1*, is known and it regulates variation in beak shape (*15*), which was not associated with survival in 2004–2005.

We performed a genome-wide screen for loci affecting overall body size in six species of Darwin's finches that primarily differ in size and size-related traits: the small, medium, and large ground finches, and the small, medium, and large tree finches (Fig. 1, A and B, and table S1). Ground finches and tree finches diverged about 400,000 years ago and exhibit ongoing gene flow within and between the two groups (*15*). By combining species of similar size in different taxa, we minimized phylogenetic effects when contrasting the genomes of species differing in size. We then genotyped individuals of the Daphne population of medium ground finches that succumbed or survived during the drought of 2004–2005. This approach allowed us to identify a locus with major effect on beak size variation that played a key role in the character displacement episode.

We sequenced 10 birds from each of the six species (total 60 birds) to  $\sim 10\times$  coverage per individual, using  $2 \times 125$ -base pair paired-end reads. The sequences were aligned to the reference genome from a female medium ground

<sup>1</sup>Department of Medical Biochemistry and Microbiology, Uppsala University, Uppsala, Sweden. <sup>2</sup>Department of Ecology and Evolutionary Biology, Princeton University, Princeton, NJ, USA. <sup>3</sup>Department of Animal Breeding and Genetics, Swedish University of Agricultural Sciences, Uppsala, Sweden. <sup>4</sup>Department of Veterinary Integrative Biosciences, Texas A&M University, College Station, TX, USA.  
\*Corresponding author. Email: leif.andersson@imbim.uu.se

## The 3.8 Å resolution cryo-EM structure of Zika virus

Devika Sirohi, Zhenguo Chen, Lei Sun, Thomas Klose, Theodore C. Pierson, Michael G. Rossmann, and Richard J. Kuhn

Science, 352 (6284), .  
DOI: 10.1126/science.aaf5316

### Unveiling the Zika virus

The ongoing Zika virus epidemic is of grave concern because of its apparent links to congenital microcephaly and Guillain-Barré syndrome. Sirohi *et al.* present a near-atomic-resolution structure of mature Zika virus determined by cryo-electron microscopy. The structure is mainly similar to that of other flaviviruses such as dengue virus; however, there are differences in a region that may be involved in binding to host receptors. The structure provides a foundation for analysis of the antigenicity and pathogenesis of Zika virus.

Science, this issue p. 467

### View the article online

<https://www.science.org/doi/10.1126/science.aaf5316>

### Permissions

<https://www.science.org/help/reprints-and-permissions>